Temperature-resolved SAXS studies of morphological changes in melt-crystallized poly(hexamethylene terephthalate) and its melting upon heating

Ya-Sen Sun*

National Synchrotron Radiation Research Center, 101 Hsin-Ann Road, Hsinchu Science Park, Hsinchu 30076, Taiwan

Abstract

Temperature-resolved small-angle X-ray scattering (SAXS) on poly(hexamethylene terephthalate) (PHT) samples crystallized from the melt yields direct information about the morphological changes in lamellar crystals and interlamellar amorphous layers upon melt-crystallization and subsequent heating to melting. Absolute intensities of these SAXS patterns were further analyzed via one-dimensional correlation and interface distribution functions. These analyses indicate that melt-crystallization at low temperature produces lamellar crystals having diverse thicknesses whereas crystallization at high temperature tends to favor growth of thick lamellar crystals with a nearly uniform distribution of thickness. When heating the PHT samples in the melting temperature region, the melting of the lamellar crystals was found to correlate well with the sequential-melting features. When these crystals are heated to higher temperatures, structural alterations from stacked lamellae to isolated lamellar crystals evolve with increasing extent of sequential melting, but, upon re-crystallization during extended annealing, the isolated lamellar crystals can pass through a reversible transition back to stacked lamellae.
© 2006 Elsevier Ltd. All rights reserved.

Keywords: Temperature-resolved SAXS; Poly(hexamethylene terephthalate); Sequential melting

1. Introduction

The melting behavior [1–3] and polymorphism [4–7] in isothermally melt-crystallized or solvent-treated poly(hexamethylene terephthalate) (PHT) have been studied extensively. Upon completion of melt-crystallization, PHT possesses two crystalline cell forms depending on thermal histories, designated as α- and β-forms [4–6]. According to conventional nomenclature for crystal forms, the α-form comprises polymer chains packed in a monoclinic unit cell, whereas the β-form has triclinic packing [4]. Complex melting peaks (two or three) are often seen in some terephthalic polyesters, such as poly(ethylene terephthalate) (PET) [8–11], poly(trimethylene terephthalate) (PTT) [12,13], poly(butylene terephthalate) (PBT) [14–18], and poly(pentamethylene terephthalate) (PPT) [19–20]. Notably, PHT, with six methylenes between the terephthalate groups, has been recently shown to exhibit an even greater number of up to six melting peaks [2,3]. In addition to the obvious presence of polymorphic crystals, the more complex multiple-melting behavior can be generally attributed to the presence of various crystallites (variations in the crystal lattice, lamellar thickness or spherulitic texture) simultaneously coexisting in PHT upon melt-crystallization. Certainly and additionally, it cannot be ruled out that reorganization of initial crystallites into thicker or different crystallite forms upon extended annealing or within a long time frame of scanning (e.g., extremely slow scan rates) [1–3]. Probing finer details and further understanding require still further investigation.

Despite strenuous efforts to clarify the multiple-melting behavior of PHT observed during heating in a differential scanning calorimeter (DSC) and their origins with respect to

* Tel.: +886 3 578 0281x7331; fax: +886 3 578 3813.
E-mail address: yssun@nsrrc.org.tw

the known polymorphism in PHT, however, much still remains yet unknown for plausibly interpreting the complex six melting peaks in PHT. Because the melting point of crystallites is supposed to be inversely related to their thicknesses, the occurrence of multiple-melting features in a semicrystalline polymer indicates that the various crystallites, other than those formed during scanning, must have varied sizes; they might also possess varied stability or meta-stability, which yields a sequential display within a temperature range in DSC [21,22].

Small-angle scattering of X-rays (SAXS) from a high-brilliance synchrotron can offer an ideal tool to record the evolution of lamellar structures during the melting process [23]. A distinct interference (or diffraction) maximum is usually observed in SAXS profiles for semicrystalline polymers consisting periodical lamellar stacks. Subsequent melting of the lamellar crystals upon heating may result in variations in position, intensity and shape of the interference maximum. Generally, three fundamentally different melting mechanisms: surface melting [24], sequential melting [25,26], and stack melting [27], have been proposed to explain the changes in the interference maximum. A model for surface melting indicates that polymer melting begins homogeneously from the basal surface of the crystalline layers [24]. As a decrease in crystalline layers for surface melting compensates an increase in the amorphous layers, the interference maximum is expected to remain constant at its original position with ignoring the temperature effect upon the differences in density between amorphous and crystalline regions [28,29]. According to a sequential-melting model, polymer melting is related to selective melting of individual lamellar crystals within a stack — a so-called lamellar bundle — according to stability [25,26]; this process reveals one characteristic feature of SAXS. Namely, monotonic scattering, known also as diffuse scattering, originating from randomly isolated lamellar crystals is present before the final stages of melting [28,29]. In contrast, according to a model for stack melting, lamellar stacks within a spherulite melt successively depending on the stability of the stacks at varied temperatures. A common representative of SAXS characteristic features is complex variations in position and intensity of the interference maximum as a consequence of the removal of entire stacks from the average scattering signal during melting, depending on the distribution of long period and crystal thickness from stack to stack [29—31].

From a theoretical point of view, Crist proposed that varied melting behavior has correspondingly varied effects on SAXS features [28,29], but no melting mechanism mentioned above describes satisfactorily the experimental SAXS features in most practical cases of polymer melting. As crystallites formed at low temperatures are thin and less stable, subsequent melting might involve much reorganization or lamellar thickening of less stable crystallites within the duration of scanning or upon extended annealing. Incorporation of reorganization within melting typically complicates the morphological parameters.

In this work, we used temperature-resolved SAXS tentatively to examine correlations between SAXS patterns and melting of PHT; we propose that a sequential-melting mechanism is likely for PHT crystallites exhibiting disparate melting points. We observed a large increase in the long period L with rising temperature during melting upon heating, which reveals an inconsistency with a theoretical argument of a nearly constant long period during sequential melting [28,29]. We attempted to acquire an enhanced understanding of attendant processes by examining SAXS features of PHT and interpretation of its complicated melting behavior.

2. Experiments

2.1. Materials

PHT was synthesized using butyl titanate as catalyst according to the method reported earlier [32,33]. The weight-average molecular weight (M_w) and polydispersity index (PDI) measured by gel permeation chromatography (GPC) are 13,800 g/mol and 2.0, respectively. At this M_w, maybe the mechanical properties are on lower sides, but its thermal properties (T_g, T_m, etc.) are expected to be characteristic of a polymer. Some of thermal transition temperatures in this PHT may be slightly lower than a longer-chain PHT, but the characteristic of crystals, multiple-melting peaks remained almost the same as those in longer-chain PHT. The melting temperature of the synthesized PHT was characterized using DSC, and the value is 144.5 °C [33].

2.2. Differential scanning calorimeter

The melting behavior of the PHT samples were investigated using a differential scanning calorimeter (DSC-7, Perkin—Elmer) equipped with a mechanical intracooler under nitrogen purge to ensure minimal sample degradation. Temperature and heat flow calibrations were done using indium and zinc. Data were collected and analyzed by using Pyris software (Perkin—Elmer). For melt-crystallization treatments, samples were first melted at 180 °C for 10 min and quickly cooled at a rate of −320 °C/min to designed isothermal temperatures (90—140 °C). For determining the transition temperatures, a dynamic heating rate of 10 °C/min was used.

2.3. SAXS measurement

Before SAXS characterization, all PHT samples were subjected to isothermal melt-crystallization at various temperatures in DSC. Temperature-resolved SAXS was employed to characterize the crystalline lamellar morphology of the crystallizing PHT, whose thickness is 1 mm each. SAXS experiments were performed at BL01B SWLS beamline at the National Synchrotron Radiation Research Center (NSRRC) (Hsinchu, Taiwan). More detailed information about the SAXS apparatus has been shown elsewhere [34]. The incident X-ray beam was focused vertically by a mirror and monochromated to the energy of 10.5 keV by a germanium (111) double-crystal monochromator, and the wavelength of the X-ray beam was $\lambda = 0.1181$ nm. The sample-to-detector

distance was 1571 mm in length. The beam stop was a round tantalum disk of 4 mm in diameter. SAXS data were collected with a one-dimensional position-sensitive detector (PSD), and the sensitivity of the PSD was calibrated by using a ^{55}Fe source before data collection. The calibration of the detector channels in terms of scattering vector was made by linear regression over the positions of numerous orders of the long period of silver behenate as the standard, with q_{max} being 1.076 nm^{-1}. The intensity profiles were output as the plot of scattering intensity (I) vs. scattering vector, q ($q = (4\pi/\lambda)\sin(\theta/2)$, where θ is the scattering angle). A calibration standard, polyethylene (PE) of 1.89-mm thickness, was used to correct the SAXS data in order to gain absolute intensity after background (air scattering) subtraction. We use the stable scattering peak of the PE, $I(q) = 36.6$ cm^{-1} at $q = 0.23$ nm^{-1}, to obtain the scaling constant between the measured $I(q)$ and the calibrated $I(q)$ [34]. Then the scaling constant can be applied to PHT samples for the absolute intensity scale. All temperature-resolved SAXS measurements were carried out at several temperatures on a hot-stage under a dry nitrogen atmosphere. The specimens were in a sample-cell sealed by two pieces of Kapton film. After the sample reached the target temperature 0.5 min was awaited for thermal equilibrium. Then, the scattering signal was acquired for 2 min.

2.4. Analysis of SAXS data

One may consider that the scattering objects are periodical stacks consisting of alternate lamellar crystals and amorphous layers. The detailed parameters of lamellar structures, such as long period (L), thickness of amorphous layers (l_a) and thickness of crystalline layers (l_c) can be extracted from SAXS profiles via a combination of the one-dimensional correlation and interface distribution functions [35–38]. The scattering intensity $I(q)$ can be related to the normalized one-dimensional correlation function, defined as [35]:

$$\gamma(r) = \frac{2\pi^2}{Q} \int\limits_0^\infty I(q)q^2 \cos(qr) \mathrm{d}q \qquad (1)$$

where r is the direction perpendicular to the surfaces of the lamellae, along which the electron density is measured. $\gamma(0) = 1$ at $r = 0$; Q is just the scattering invariant:

$$Q = \frac{1}{2\pi^2} \int\limits_0^\infty I(q)q^2 \mathrm{d}q \qquad (2)$$

Provided that whole sample is homogeneously filled with stacks of lamellae, the invariant can be directly proportional to the volume fraction of the crystallites ϕ_c, by:

$$Q = \phi_c(1 - \phi_c)\Delta\rho_e^2 \qquad (3)$$

here $\Delta\rho_e$ denotes the electron density contrast between the crystalline and amorphous layers.

In the case of an ideal two-phase model with sharp boundaries at the crystal/amorphous interface, the Porod's law can be given to describe the asymptotic behavior of the background-subtracted SAXS curves at the large q region [39]:

$$\lim_{q \to \infty} I(q) = K_p \frac{\exp(-\sigma^2 q^2)}{q^4} + I_{fl} \qquad (4)$$

Hereby K_p is the Porod constant and σ is the thickness of the sigmoidal-gradient electron density transition layer of crystal/amorphous interface and I_{fl} is the background intensity resulting from thermal density fluctuations. The second derivative of the correlation function, $\gamma''(r)$, shows the distribution of distances between interfaces [37,39]:

$$\gamma''(r) \approx \Delta\rho_e^2[h_c(r) + h_a(r) - 2h_{ac}(r) + h_{aca}(r) + h_{acc}(r) + \ldots] \qquad (5)$$

Of main important are the first three terms of $\gamma''(r)$. They give the most probable morphological parameters related to a series of distribution functions of the thicknesses of the crystalline (h_c) and amorphous layers (h_a), and sum of both (h_{ac}), in which h_{ac} reflects, in other words, the size distribution function of long period L [40].

3. Result and discussion

3.1. Isothermally crystallized PHT

For melt-crystallization, PHT samples were first held in the melt at 180 °C for 10 min, then quenched to one of the pre-setting temperatures ($T_C = 90, 100, 110, 120, 130$ and 140 °C) and isothermally crystallized at the temperatures for long periods until melt-crystallization was done in DSC. Experimentally, after the melt-crystallization, the crystalline structures in the melt-crystallized PHT specimens were characterized by using temperature-resolved SAXS. The SAXS profiles for the crystalline structures in PHT were recorded at 25 °C first. Because a SAXS profile can exhibit a significant dependence on temperature [41], we acquired SAXS profiles also at the corresponding temperature of melt-crystallization for each melt-crystallized PHT specimen. In comparison with Lorentz-corrected SAXS profiles as shown in Fig. 1, the patterns were recorded at 25 °C and elevated temperatures. The scattering profiles in the figure are given in absolute units and multiplied by the Lorentz factor q^2; the Lorentz-corrected absolute intensities of the profiles are successively shifted upward one decade from bottom to top. The Lorentz-corrected SAXS profiles show that the melt-crystallized PHT samples exhibit an interference maximum overlapped with a shoulder (indicated by thick arrowheads) in the q range of 0.2–0.8 nm^{-1}. This result indicates a typical characteristic of periodical lamellar structures consisting of alternate crystalline and amorphous layers. The lamellar structures appear to exist in PHT when subjected to melt-crystallization at various isothermal temperatures (90–140 °C). With increasing T_C, the interference maximum shifts toward smaller q. Upon
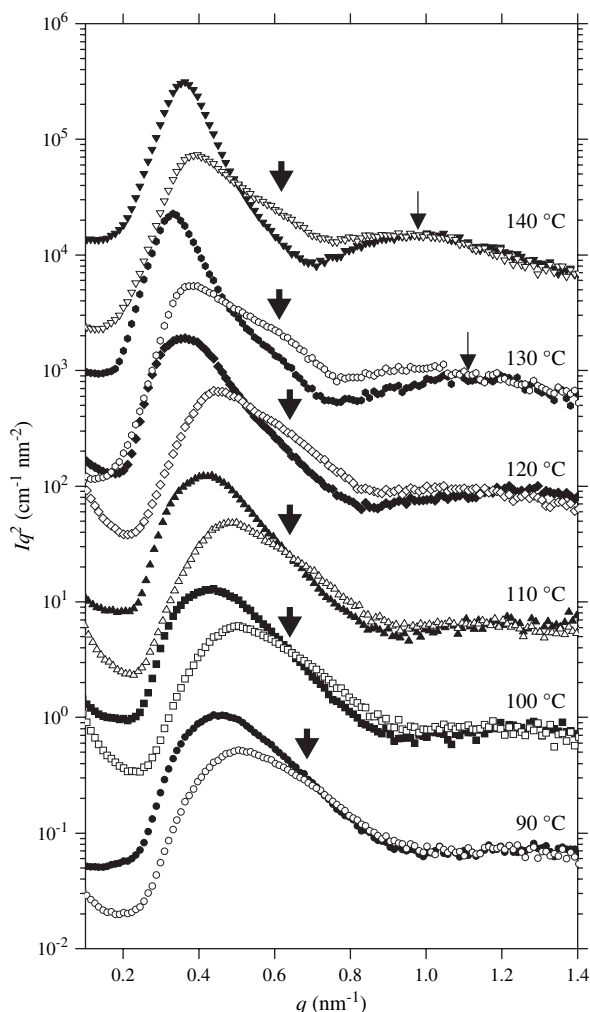
Fig. 1. Lorentz-corrected SAXS profiles for a series of PHT samples, melt-crystallized at temperatures between 90 and 140 °C (temperature is labeled on individual traces), recorded at 25 °C (open symbols) and corresponding crystallization temperatures (solid symbols).

crystallization at temperatures equal to or greater than 120 °C, an additional broad hump, indicated by thin arrowheads, emerges in a region for $q > 0.8$ nm^{-1}, where its intensity becomes increasingly evident with further increasing T_C.

For lamellar structures of the melt-crystallized PHT samples examined at elevated temperatures, corresponding to T_C, the interference maximum shifted toward small q and its integrated intensity became enhanced. Thus, varying the measurement temperature for SAXS characterizations results in varied signal intensity and position of the interference maximum. As expansion coefficients of the crystalline and amorphous layers differ [41], this variation in the interference maximum can be considered to be due to the greater contrast of electron density between the two phases at the elevated temperatures. On the other hand, the hump remains nearly constant in peak position. Accordingly, we attribute this hump to a first-order particle scattering from the isolated lamellar crystals with a nearly uniform distribution of thickness. $P(q)$ is the average form factor resulting from the scattering of isolated lamellar crystals

on assumption of a Gaussian distribution of thickness, and is given by [42]:

$$P(q) = \int_{z=0}^{\infty} p_c^2(q) h_c(z) \mathrm{d}z \Big/ \int_{z=0}^{\infty} h_c(z) \mathrm{d}z \qquad (6a)$$

in which $p_c^2(q)$ is the form factor for a single lamella and $h_c(z)$ is the distribution function for the particle thickness z; their relation to the average thickness l_c and the thickness deviation σ_c of z is:

$$p_c^2(q) \approx \left(\frac{\sin(qz/2)}{(qz/2)}\right)^2 \exp(-q^2 \sigma^2) \qquad (6b)$$

$$h_c(z) = \left(2\pi\sigma_c^2\right)^{-1/2} \exp\left[-(z - l_c)^2 / 2\sigma_c^2\right] \qquad (6c)$$

The interference maximum is also qualitatively described on employing a structure factor in terms of a one-dimensional paracrystalline structure [42,43]. For Gaussian distributions for stacks of lamellae with a long period L and a standard deviation (σ_D) of the long period, the structure factor for periodical lamellar structures is given by:

$$S(q) = \frac{\sinh\left(q^2 \sigma_D^2 / 4\right)}{\cosh(q^2 \sigma_D^2 / 4) - \cos(qL)} \qquad (7)$$

In the case of periodical lamellae stacks with a sharp distribution of crystal thickness, the theoretical intensity profile $I(q)$ for the lamellar structure is the product of structure factor and form factor, simply presented as [42]:

$$I(q) = S(q)P(q) \qquad (8)$$

Schematic (A) of Fig. 2 shows an example from a SAXS profile collected at 25 °C for a PHT sample melt-crystallized at 140 °C. Comparison of the calculated particle-scattering profile with the experimental profile reveals that the broad hump centered about $q = 1.0$ nm^{-1} (indicated by an arrowhead) is associated with the first-order scattering hump from isolated lamellar crystals with a nearly uniform distribution of thickness, whereas the interference maximum located near $q = 0.4$ nm^{-1} is a characteristic diffraction feature of the periodic stacks of lamellae. The substantially mutual interference between the intensity of the structure factor and that of the form factor at small q produces a clear maximum at a finite q (see the filled-circle curve for theoretical $I(q)q^2$). For $q \geq 0.6$ nm^{-1}, the stacks show a poor order so that the oscillation of the long periods in the q range is strongly attenuated. The first-order particle scattering for the lamellar crystals in the q range can be well described by Eq. (6a–c). Schematic (B) displays experimental SAXS curves and theoretical particle-scatterings for PHT samples melt-crystallized at 120, 130 and 140 °C. Theoretically fitted curves from SAXS patterns collected at 25 °C yield average thickness values (specified in the caption of Fig. 2) of the lamellar crystals. Therefore, for PHT specimens melt-crystallized in the temperature region 90–110 °C, the absence of the hump is explicable in terms of
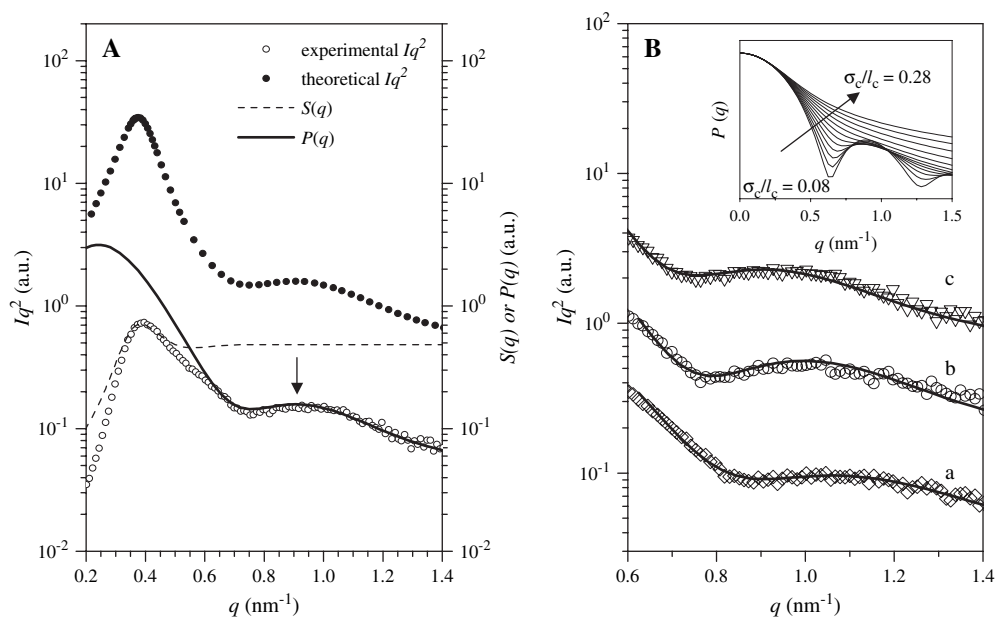
Fig. 2. (A) Comparison of the experimental $I(q)q^2$ (open circles) with theoretic fits for $P(q)$ (thick line), $S(q)$ (dashed line) and theoretic $I(q)q^2$ (filled circles), and (B) fits of observed scattering, for which the calculated results are depicted with solid lines and the experimental profiles are represented by open symbols, of PHT samples crystallized at (a) 120 ($l_c = 4.37$ nm, $\sigma_c = 0.77$ nm), (b) 130 ($l_c = 4.67$ nm, $\sigma_c = 0.81$ nm) and (c) 140 °C ($l_c = 5.05$ nm, $\sigma_c = 0.80$ nm). The inset shows the normalized deviation-dependence of the form factor scattering derived theoretically.

the smearing of the form factor consequent upon the presence of lamellar crystals having widely variable thicknesses. Melt-crystallization at temperatures above 120 °C tends to favor greater fractions of lamellar crystals with a nearly uniform distribution of thickness. The homogeneous lamellar crystals were generated when PHT was melt-crystallized at temperatures ≥ 140 °C, as evidenced by single endotherm upon scanning in DSC [2,3]. This appearance of the broad hump can thus be considered to indicate the existence of lamellar crystals of PHT with a nearly uniform distribution of thickness. The dependence of the first-order scattering (hump) on the normalized standard deviation, namely σ_c/l_c (from 0.08 to 0.28), was qualitatively described with the theoretical form factor of the crystalline layers with an average thickness $l_c = 5.05$ nm (Eq. (6a–c)). For lamellae having greatly varying thicknesses according to a large value of σ_c/l_c, the first-order scattered hump broadens and smears. By contrast, for lamellae having a nearly uniform distribution of thickness according to a small σ_c/l_c, the first-order scattered hump narrows and becomes discernible.

Furthermore, for PHT samples melt-crystallized at temperatures above 120 °C, arising measurement temperature leads to increases in intensity at q regions close to the origin and shifts the interference maximum toward low q-values. Such a feature is partly attributed to the melting of few thin crystallites. The thin crystallites may form via a further "secondary" crystallization during a subsequent cooling to room temperature [36]. Particularly, if the isothermal crystallization rate at high T_C is very slow, the crystallization may remain incomplete after the certain time period allowed for completion of an isothermal crystallization at low T_C. Consequently, a subsequent cooling to room temperature leads to the formation of

new thin crystallites. The thermal stability of the thin crystallites is lower than that of the isothermally crystallized lamellae. Because we recorded the SAXS data at T_C, the lamellar crystals formed at the T_C are expected to be resistant to melting and to remain unmelted. However, the thin crystallites may melt into liquid states. To examine such a hypothesis, we sought further evidence and performed more detailed analyses. It is instructive to scrutinize the morphological parameters given by the one-dimensional correlation $\gamma(r)$ and interface distribution $\gamma''(r)$ functions. Fig. 3 reveals the functions $\gamma(r)$ (schematic (A)) and $\gamma''(r)$ (schematic (B)) calculated for these melt-crystallized PHT samples. The functions $\gamma(r)$ presented in schematic (A) in many instances clearly exhibit the maxima and minima. The long period L can be determined from the position of the first maximum in $\gamma(r)$. A large increase in L was found when the lamellar structures for each melt-crystallized PHT sample were examined at the corresponding temperature of melt-crystallization. The first minimum might correlate with either l_c or l_a. Therefore, an assignment of the first minimum relies on further knowledge such as bulk crystallinity by thermal analysis. According to a premise that stacked lamellae are volume-filling in the semicrystalline polymers, the linear crystallinity (ϕ_c) determined by SAXS is identical to the bulk crystallinity (ϕ_c^{bulk}) measured by thermal analysis. When the bulk crystallinity is lower than 0.5, the first minimum represents l_c. By using the value of 144 J/g for the melting enthalpy of 100% crystalline PHT proposed by Lefèbvre et al. [1], the bulk crystallinity ϕ_c^{bulk} for all the studied PHT samples was less than 50% based on the data of heat of fusion as measured by DSC scanning on the melt-crystallized PHT samples [3]. Indeed, it is reasonable to assign the first minimum as l_c.
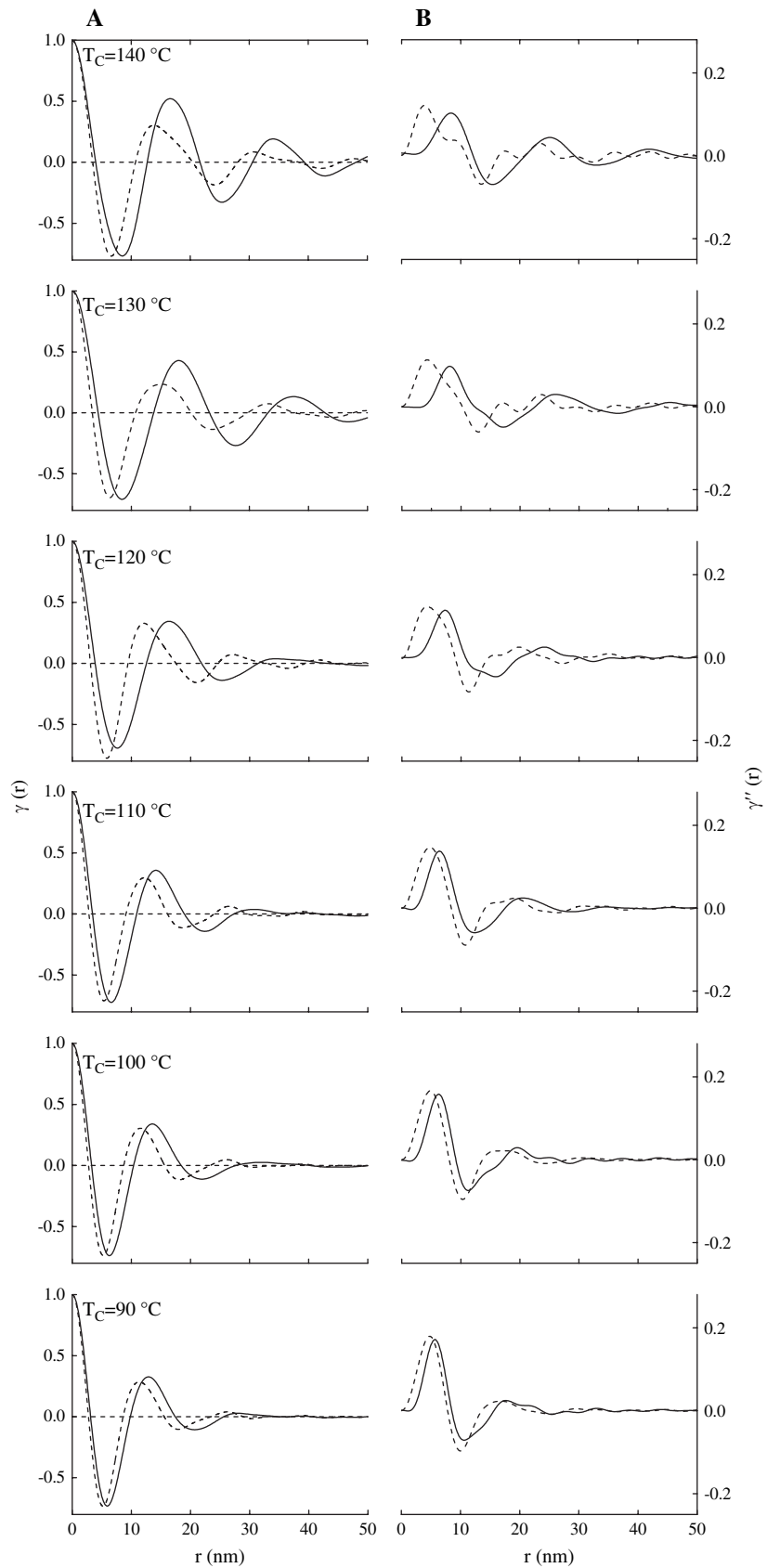
Fig. 3. (A) One-dimensional correlation and (B) interface distribution functions, in which dashed-line curves indicate the functions calculated from the open-symbol profiles, and solid-line curves display the functions calculated from the solid-symbol profiles in Fig. 1.

For the 90 °C-crystallized PHT sample, the small increases in L and l_c with rising measurement temperature indicate that the lamellar crystals almost formed at 90 °C. A subsequent cooling could not bring about the new generation of thin crystallites. By contrast, the large increases in L and l_c for the 120, 130 and 140 °C-crystallized PHT samples are observed if the measuring temperature is at the corresponding T_C. This result suggests that such an effect of temperature on structural parameters is more likely upon partial melting of lamellae [36]. Fig. 3(B) shows the functions $\gamma''(r)$ derived from the same curves as in the case of Fig. 1. As shown in schematic (B), for the PHT specimens melt-crystallized in the temperature region 90–110 °C, the first maximum in $\gamma''(r)$ is undoubtedly assigned as the crystalline distribution function (h_c) according to its position. Determination of long period L is realized by locating the position of the first minimum in $\gamma''(r)$. For the PHT samples melt-crystallized at high T_Cs (120, 130 and 140 °C), the functions $\gamma''(r)$, derived from the SAXS profiles collected at room temperature, are complicated. The first two maxima of $\gamma''(r)$ may be a superposition of three contributions – two peaks from the distribution functions of the crystalline crystals (h_c) and amorphous layers (h_a), respectively, and one inverted peak from the distribution one (h_{ac}) of the long period L (see Eq. (5)) [37]. Therefore, which of the two positive features is due to h_c and which to h_a is indistinguishable. Nevertheless, rising measuring temperature would lead to the functions $\gamma''(r)$ with single first maximum, suggesting that the variances in structural parameters are more likely attributed to partial melting of lamellae. The behavior of partial melting is describable in terms of a continuous decrease of crystallinity, as a consequence of successive melting into liquid states from a crystalline state (cf. next section).

3.2. Subsequent melting

The thermal behavior of melt-crystallized PHT is complicated. The multiple-melting endotherms were found upon scanning 90 °C-crystallized PHT sample in a DSC [3]. The essential features observed are recalled here since they partly connect with the present study [3]. As shown in schematic (A) of Fig. 4, the DSC trace displays five distinct endotherms, labeled as P_1, P_2, P_3, P_4 and P_5 (from low to high temperature). The lamellar crystals corresponding to each of these five melting peaks are briefly called P_1, P_2, P_3, P_4 and P_5 lamellar crystals. Moreover, two exotherms (crystallization peaks) are distinctly visible trailing the melting of P_1 and P_2. In order to detect morphological changes during a subsequent melting, we carried out SAXS experiments at different temperatures in the melting range of the PHT crystallites. After the completion of melt-crystallization at 90 °C for 2 h, the lamellar structures were examined at 90 °C for comparison and then subjected to various temperatures in the melting region to examine relationships between lamellar structure and melting behavior. Schematic (B) of Fig. 4 exhibits the Lorentz-corrected SAXS profiles as a function of temperature, in which the Lorentz-corrected absolute intensities of the profiles are successively shifted upward one decade from bottom to top with respect to curve-a and
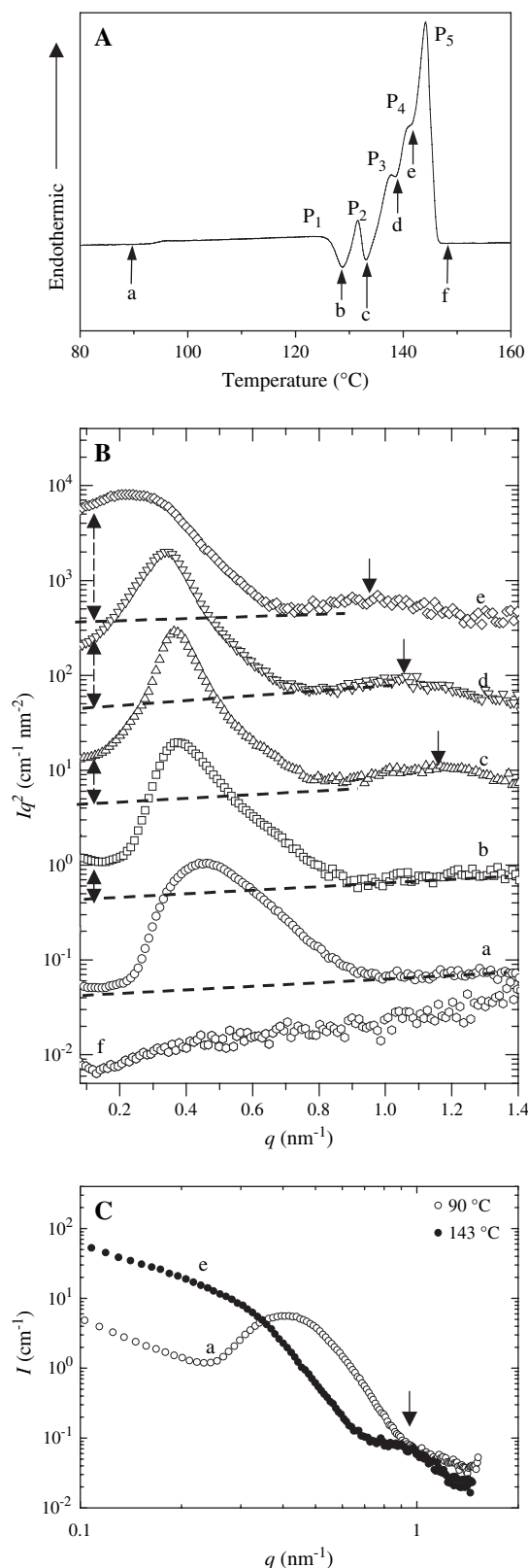
Fig. 4. (A) DSC thermogram (heating rate = 10 °C/min) of PHT melt-crystallized at 90 °C for 120 min, (B) Lorentz-corrected SAXS profiles for the 90 °C-crystallized PHT subjected to subsequent heating at (a) 90, (b) 127, (c) 132, (d) 137, (e) 143 and (f) 148 °C, and (C) two SAXS profiles in absolute intensity, as collected at (a) 90 and (e) 143 °C, respectively.

curve-f. Curve-a reveals one broad interference maximum at $q = 0.455$ nm^{-1} for the originally lamellar structure developed at the initial crystallization of 90 °C. Further heating at 127 °C to eliminate the P_1 crystals, the interference maximum sharpens and its position moves toward low q-values (curve-b). At 132 °C corresponding to the end of the melting of P_2 (curve-c), the interference maximum retains constant in position, accompanied by the appearance of a small hump (at $q = 1.1$ nm^{-1}). Upon heating the PHT sample to 137 and 143 °C (P_3 and P_4 lamellar crystals melt in sequence from low to high temperature), the overall intensity distribution shifts to very low q regions (highlighted by double-arrowhead, curve-d and curve-e). The interference maximum at $q = 0.368$ nm^{-1} reveals a significant depression in peak intensity at the end of the melting of P_4, suggesting that the interference maximum is nearly destroyed. In other words, most of the lamellar crystals in PHT (P_1-, P_2-, P_3- and P_4-type lamellar crystals) melt successively according to their melting temperatures upon heating the PHT sample at temperatures from 120 to 143 °C. The lamellar crystals (P_5 crystals) of more uniform thickness remain and distribute randomly in PHT at the end of the melting of P_4 lamellar crystals, which gives rise to the monotonic scattering with the first interference maximum being absent (curve-e). Upon destruction of periodic stacks of lamellae for PHT at 143 °C, the monotonic scattering at very low q becomes more evident at the expense of disappearing of the structure factor (i.e., the interference maximum). Further heating leads to an abrupt decrease of intensity until final melting at $T = 148$ °C (curve-f), indicative of a homogeneous liquid state as a consequence of complete melting of all PHT lamellar crystals.

From the SAXS profiles at different temperatures, we proposed that the melting process for the PHT lamellar structures fits the sequential melting [28,29]. Such an argument is supported by the appearance of the monotonic scattering accompanied with single particle scattering instead of an interference maximum before the end of the melting range. The monotonic scattering has been found in a few experimental treatments for semicrystalline polymers, such as syndiotactic polypropylene [44], polyethylene [45–47], poly(3-hydroxybutyrate) [48], and poly(ethylene naphthalene 2,6-dicarbonate) [49], and in various other extensive theoretical treatments [28,29]. For better showing the lamellar evolution with varying temperature, two SAXS patterns in absolute intensity, recorded at 90 and 143 °C, respectively, were shown in Fig. 4(C). In Fig. 4(C), a close examination of the absolute intensity of curve-e indicates that the maximum in the single particle intensity at $q = 1$ nm^{-1} is three orders of magnitude smaller than the monotonic scattering located at q region close to the origin. Comparison between curve-a and curve-e indicates that the monotonic scattering grows at the expense of reduction of the interference maximum.

In modeling the melting of the PHT crystallites, an evolution of the lamellar structures in PHT as a function of temperature upon heating was further explored by the corresponding one-dimensional correlation $\gamma(r)$ and interface distribution functions $\gamma''(r)$, as illustrated in Fig. 5 (schematics (A) and (B)). Schematic (A) of Fig. 5 reveals the functions $\gamma(r)$ for
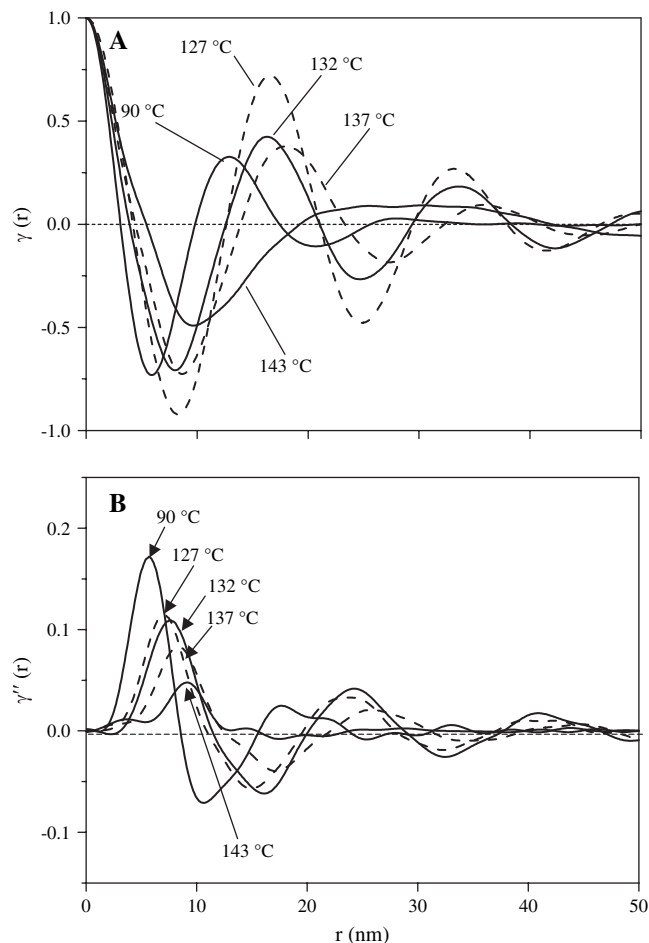
Fig. 5. (A) One-dimensional correlation and (B) interface distribution functions of 90 °C-crystallized PHT subjected to subsequent heating at 90, 127, 132, 137 and 143 °C.

90 °C-crystallized PHT at various temperatures. After the melting of P_1 upon heating the 90 °C-crystallized PHT at 127 °C, there is an obvious re-crystallization, as evidenced by the enhanced magnitude of the first minimum and maximum and also by shifting in positions of both toward high distance. The value of the correlation function at the first minimum is related to the ratio of the volume fraction (ϕ_c) of the crystalline layer to that (ϕ_a) of the amorphous layer [35]. Upon melt-crystallization on PHT at a low temperature 90 °C the P_1 lamellar crystals in PHT possess thinnest thickness and much less thermal stability. During heating it is likely that the thinnest lamellae melted and subsequently re-crystallized into the thick ones. The crystallinity may increase slightly or remain constant upon melting/reorganization of the imperfect lamella if the loss in crystallinity due to the melting of the thinnest lamellae is compensated for the increase in crystallinity given by the reorganized thick crystallites upon re-crystallization [3]. Thus, the conspicuous increase in the magnitude of the first minimum can be ascribed to an event of the reorganization of lamellar crystals upon melting/re-crystallization during a heating, which is in excellent agreement with an observation for an exothermic peak at ~5 °C above the endothermic peak of P_1 lamellar crystals

in the DSC trace. In fact, reorganization after melting may start with high crystal growth rates and then slows down progressively with the advanced extent of melting upon heating to high temperatures [44]. Thus, the crystallinity value remains unchanged (or increases slightly) in the beginning of the melting of P_1 lamellar crystals but gradually decreases with further rising temperature. The decreased crystallinity is due to the fact that continuous heating to high temperatures causes more of the lamellar crystals to melt into liquid states and meanwhile limits the extent of reorganization. Further melting upon heating the PHT sample at 143 °C brought about the significantly suppressed maxima and minima in $\gamma(r)$. This suggests that a great amount (P_1–P_4) of the lamellar crystals melt into liquid states upon further heating to 143 °C and the remaining P_5 lamellar crystals randomly distribute in PHT.

Schematic (B) of Fig. 5 shows that the most noticeable depression of lamellar stacks upon sequential melting can be seen in the interface distribution functions $\gamma''(r)$. For the PHT crystallites formed at 90 °C, the function $\gamma''(r)$ reveals single first maximum, which has previously been ascribed to the crystalline distribution (h_c). The first maximum becomes much weaker in magnitude when partial melting for the lamellar crystals proceeds profoundly upon heating the PHT sample beyond the melting temperature of P_4 crystals (say 143 °C). Also, with increasing sequential melting upon heating the PHT sample to high temperatures, the position of the maximum shifts to larger distances gradually and the width of the crystalline distribution becomes sharper. In addition, the first minimum corresponding to the distribution function of the long period L is substantially suppressed when heating the 90 °C-crystallized PHT sample at 143 °C. These results suggest that most of the periodically stacked lamellae were destroyed via typically sequential melting and that consequently thick lamellar crystals with a nearly uniform distribution of thickness, which lack stack periodicity, remain in PHT at the end of the melting of P_4 lamellar crystals.

For PHT melt-crystallized at 120 °C, more perfect crystals develop at the initial crystallization [2,3]. It is instructive to re-examine the evolution of the lamellar structures as a function of temperature. Prior to SAXS characterization, the sample was melt-crystallized at exactly 120 °C for 2 h and immediately cooled to 25 °C. Schematic (A) of Fig. 6 reveals a corresponding DSC trace, which reveals five melting endothermic peaks (labeled as P', P_1, P_2, P_3 and P_5^* from low to high temperature) upon heating the 120 °C crystallized PHT at a scan rate of 10 °C/min [2,3]. Moreover, an exotherm (crystallization peaks) is distinctly visible trailing the melting of P_1. An additional endotherm (P') located at the temperature region below 120 °C suggests that new thin crystallites form upon a subsequent cooling after the isothermal crystallization at 120 °C. Schematic (B) of Fig. 6 reveals the Lorentz-corrected SAXS scattering profiles corresponding to the evolution of the lamellar structures at various temperatures. Curve-a shows one interference maximum located at $q = 0.363$ nm^{-1} for the PHT lamellar crystals at 120 °C. Upon heating to $T = 135$ °C corresponding to the end of the melting temperature of P_1, it was seen that the interference maximum becomes
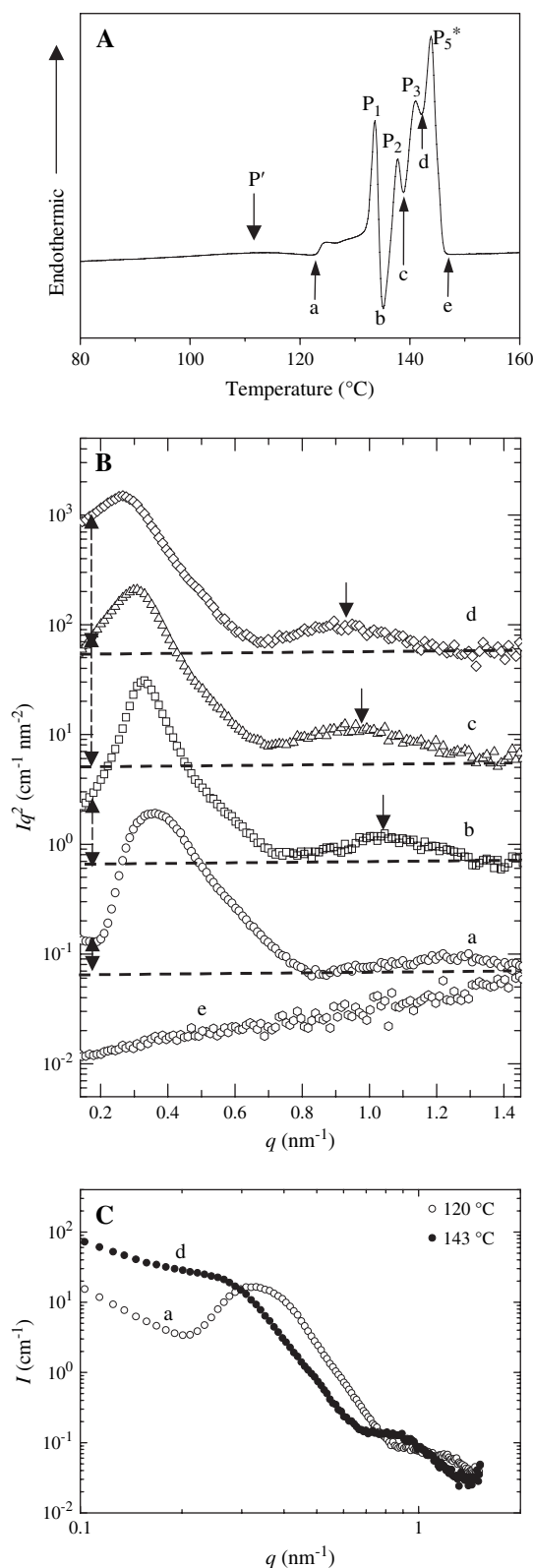
Fig. 6. (A) DSC thermogram (heating rate = 10 °C/min) of PHT melt-crystallized at 120 °C for 240 min, (B) Lorentz-corrected SAXS profiles of 120 °C-crystallized PHT subjected to subsequent heating at (a) 120, (b) 135, (c) 139, (d) 143 and (e) 148 °C, and (C) two SAXS profiles in absolute intensity, as collected at (a) 120 and (d) 143 °C, respectively.

sharpening (curve-b). Besides, one broad hump centered at $q = 1.046$ nm^{-1} (denoted by arrowhead) becomes more evident in curve-b, indicative of the lamellar crystals with a fairly uniform distribution. Further heating at T = 139 and 143 °C (curve-c and curve-d), where P$_2$- and P$_3$-type lamellar crystals melt in sequence according to thermal stability, the overall intensity distribution (marked by double-arrowhead) emerges at very lower q, accompanied by weakening of the interference maximum and shifting of the small scattered hump toward low q-values; there seems to appear a dominant contribution at very small q, while the interference peak weakens. At 148 °C (P$_5^*$ lamellar crystals melt), the disappearance of both the interference peak and scattered hump indicates that the PHT sample comprises a homogeneous melt. For better showing the lamellar evolution with varying temperature, two SAXS patterns with absolute units, recorded at 120 and 143 °C, respectively, were shown in Fig. 6(C). In comparison with curve-a, curve-d reveals that heating at 143 °C reduces the interference maximum but enhances the monotonic scattering instead. The analysis of the absolute intensity in curve-d indicates that the maximum intensity in the single particle at $q = 0.9$ nm^{-1} is ca. 0.14 cm^{-1}, and that the intensity of the monotonic scattering located at $q = 0.1$ nm^{-1} is 94.4 cm^{-1}, being three orders of magnitude larger than the observed particle-scattering intensity.

The corresponding $\gamma(r)$ and $\gamma''(r)$ functions derived from the SAXS curves in the previous figure are given in Fig. 7 (schematics (A) and (B), respectively). Schematic (A) of Fig. 7 reflects a similar trend in which the first maximum in $\gamma(r)$ gradually shifts to larger distance with increasing temperature. In particular, the melting of the P$_1$ lamellar crystals was immediately followed by reorganization, which reveals the nearly constant amplitude of the correlation function at the first minimum for the lamellar crystals at 135 °C. Further melting at 139 and 143 °C gives rise to a correlation function with the suppressed first minimum and maximum in $\gamma(r)$.

Schematic (B) of Fig. 7 shows the interface correlation functions $\gamma''(r)$. The $\gamma''(r)$ function for the lamellar crystals at 120 °C reveals first maximum. During further heating, the position of the first maximum shifts to a larger distance upon heating the lamellar crystals at 135 °C. The maximum exhibits depressed magnitude with increasing degrees of sequential melting upon heating PHT to higher temperatures and the shape of the first minimum (corresponding to the long space L) becomes weaker and distorted. The weakening of the first minimum is explained as follows. With increase in sequential melting, the position of the amorphous distribution function (h_a) may move to larger distances with temperature; also, the amorphous distribution broadens and distorts in shape [13]. When increasing the sequential melting at high temperatures, such a distorted distribution function of amorphous layers would approach and interfere with the size distribution of L, resulting in the weakening of the first minimum [13].

Although the sequential-melting model can best describe the SAXS-curve conversion from peaked (discrete) to monotonic (diffuse) scattering before the final stages of the melting [28,29], this model, however, does not coincide with the fact
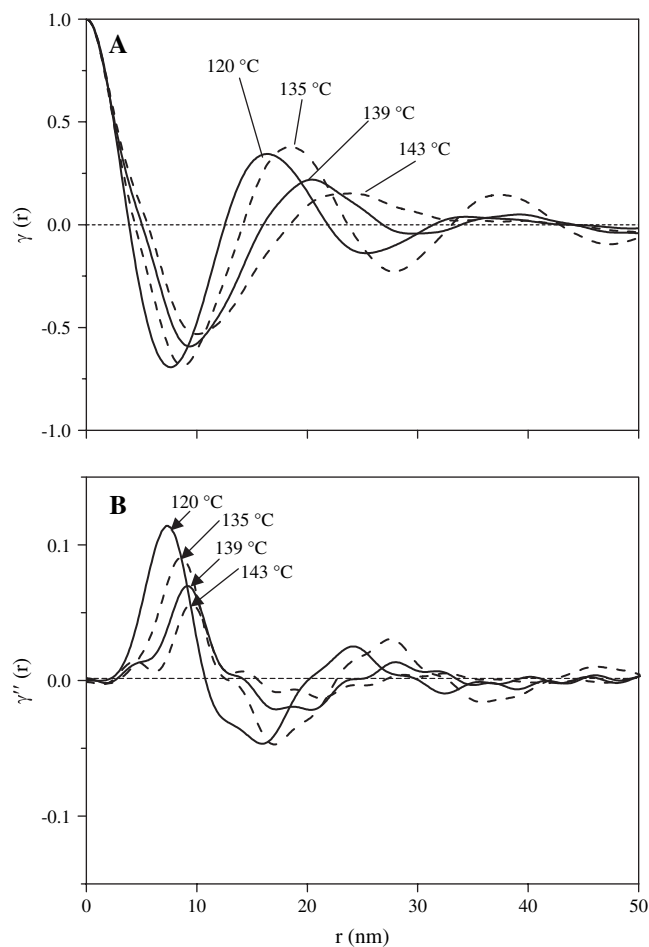
Fig. 7. (A) One-dimensional correlation and (B) interface distribution functions of 120 °C-crystallized PHT subjected to subsequent heating at 120, 135, 139 and 143 °C.

that the long period L increases with temperature. The apparent increase in L might be consistent with one of the certain characteristics of stack melting. However, as shown earlier in Fig. 7, we found that the intensity at very small q is progressively more enhanced before the final stages of the melting, as opposite to the depressed SAXS features with increases of temperature for the stack melting [28]. In other semi-rigid polymers such as poly(etheretherketone) (PEEK) [8,50–52], poly(aryl ether ketone ketone) (PEKK) [53], PET [8–11], PTT [13], and PEN [8,49,54], the mechanism of stack melting was proposed to interpret the observed increases in long period and the lamellar thickness during melting of lamellae upon heating.

In comparison with the comparatively large changes in L in the correlation functions $\gamma(r)$, the position of crystalline layers shifts slightly under the same thermal histories. In fact, the greater expansion variation of the amorphous layers with temperature is likely responsible for the changes in L during polymer melting. Successive melting of the lamellar crystals into liquid states promotes the extent of the amorphous regions, and hence a great deal of thermal expansion from the additional portions of amorphous layers upon melting gives rise to the observed increase in L [36].

Furthermore, it is known that the melting process is a first-order transition, which can occur as a discontinuity in volume [55]. That is, an abrupt increase in specific volume with temperature is found as the crystalline state melts into the liquid state. Generally a variety of lamellar crystals, which differ in thermal stability, coexist in semicrystalline polymers when melt-crystallized at low temperatures; hence melting of most polymers typically occurs over a range of several degrees or more. As the lamellar crystals within a stack melt successively into the liquid state upon heating from low to high temperature, a larger dimensional change in the amorphous layers than that in the lamellar crystals is expected. Such an increase in dimensions of amorphous layers at higher temperature is likely responsible for the increase in long period L during the sequential-melting process.

3.3. Reversibility from isolated lamella back to stacked lamella

It has been proposed that the sequential-melting process of the lamellar crystals in semicrystalline polymers in some respects is an inverse route of the crystallization, which starts with the formation of isolated lamellar crystals at the early stage of crystallization followed by the formation of stacks of lamellae [38,45,46]. For further supporting the observation that the melting process of PHT lamellar crystals is attributed to the sequential melting, another extended annealing experiment was performed with time- and temperature-resolved SAXS with a hot-stage to impose various thermal events on the sample, which was identically melt-crystallized at 130 °C for 2 h. The 130 °C-crystallized PHT was found to reveal dual melting endotherms, which further indicates at least existence of discrete and different lamellar types [2,3]. For PHT melt-crystallized at 130 °C, a greater amount of lamellar crystals with good thermal stability developed at the initial crystallization. Only upon extended annealing or within a long time frame of scanning (at extremely low scan rates), reorganization of initial crystals may be more likely [3].

Fig. 8(a–d) exhibits the Lorentz-corrected SAXS curves of PHT sample subjected to four different thermal treatments, respectively. The first sample was examined at 25 °C just after the melt-crystallization at 130 °C. Fig. 8(a) reveals a strong interference maximum combined with a broad hump in this melt-crystallized PHT. The second sample was then heated to 143 °C for melting the thin PHT lamellar crystals that correspond to the first enothermic peak at the low temperature. Upon raising temperature to 143 °C to eliminate the population of the thin lamellae, the interference maximum was significantly destroyed. Upon depression of the interference maximum, the monotonic scattering at very low q becomes evident (Fig. 8(b)). This suggests that isolated thick lamellae exist and distribute randomly in PHT after the elimination of the lamellar crystals with less thermal stability. Upon extended annealing at 143 °C for 170 min, reorganization becomes more likely, as illustrated in Fig. 8(c), which reveals clearly the interference maximum and broad hump. The interference maximum and scattering hump become more evidence with
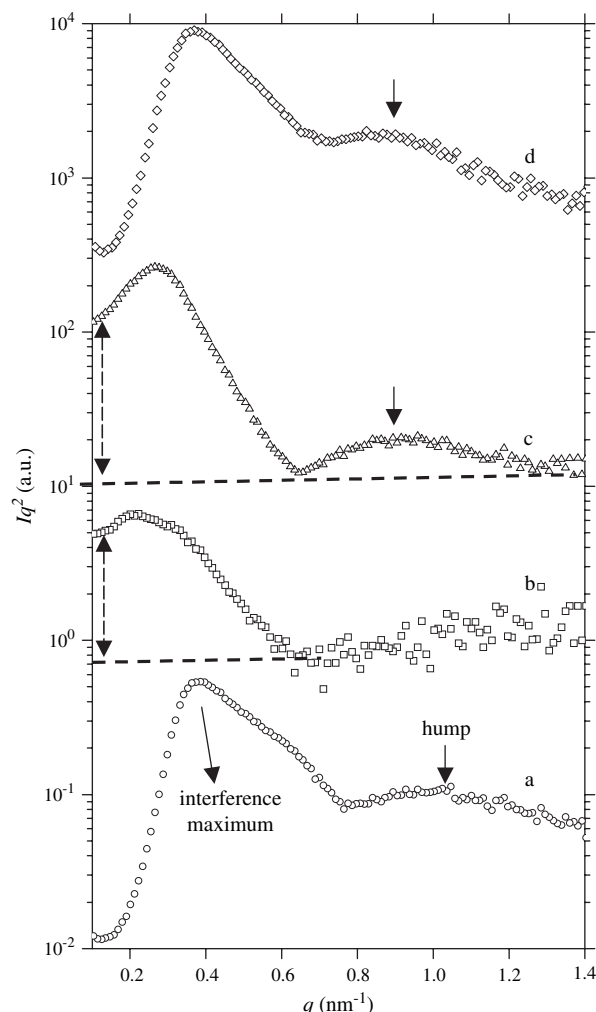
Fig. 8. Lorentz-corrected SAXS profiles for (a) PHT melt-crystallized at 130 °C for 2 h, and then subsequently post-annealed at 143 °C for (b) 5 min, (c) 170 min, and (d) 8 h. Note that the profiles (a) and (d) were collected at 25 °C.

increasing time upon annealing the first sample at 143 °C for a long time of 8 h (Fig. 8(d)), indicative of the formation of stacks of lamellae. The SAXS profiles (a) and (d) look very similar to each other. This suggests a very interesting fact that the prolonged annealing gives similar structures as formed in the original sample (melt-crystallized at 130 °C). Considering that the PHT polymer chains spontaneously recovered the similar structure from partial melting (profile (b)) upon the prolonged annealing, how fantastic the nature is.

From the Lorentz-corrected SAXS evidence shown above, it indicates that a reversible transition occurs between the stacked lamellae and isolated lamellar crystals. Melt-crystallization on PHT first produces stacked lamellae. The stacked lamellae in PHT can then be transformed into isolated lamellar crystals when the lamellar crystals are partially melted upon heating at 143 °C. If PHT is given a sufficiently long duration for re-crystallization at the temperature of 143 °C, a reversible transition back to stacked lamellae from the isolated lamellar crystals is likely to occur in a longer time scale, indicating the possibility of lamellar reorganization.

4. Conclusion

The interlamellar crystalline and amorphous layers that constitute the crystalline morphology in PHT upon melt-crystallization at various temperatures (90–140 °C) were studied using temperature-resolved SAXS. A broad interference maximum observed in the SAXS profiles for PHT melt-crystallized at the low temperatures of 90–120 °C indicates that various lamellar crystals, differing in the lamellar thickness, coexist in PHT. Higher melt-crystallization temperatures tend to favor greater fractions of thick lamellar crystals with a uniform distribution of thickness, as evidenced by the peak sharpening of the interference maximum and by the appearance of the scattering hump. As a matter of fact, the homogeneous lamellar crystals with a fairly uniform distribution of thickness became dominating species if PHT was melt-crystallized at temperatures equal to or higher than 140 °C.

Upon heating the various PHT lamellar crystals to near the melting range, distinct changes in the shape and intensity of the interference maximum were observed. The SAXS-pattern conversion was found to change from a peaked to monotonic scattering with increasing extents of melting upon increases of temperature. Such a fact suggests that the melting process for the PHT lamellar crystals proceeds via sequential melting. As a result of the suggested sequential-melting process of the PHT crystallites, the long period L indeed increases with melting temperature, which is due to greater thermal expansion in the amorphous layer than the lamellar crystal. A rise in dimensions of amorphous layers with increasing temperature is likely responsible for the increase in long period L during the sequential-melting process. Prior to the final stages of partial melting for PHT lamellar crystals, the originally stacked lamellae were found to transform into the isolated lamellar crystals upon heating to high temperatures. Furthermore, such structural change for the PHT lamellar crystals is reversible. These isolated lamellae can be reversibly transformed back to stacked lamellae upon reorganization by extended annealing for a long time.

Acknowledgments

References

[1] Lefèbvre X, Koch MHJ, Reynaers H, David C. J Polym Sci Polym Phys 1999;37:1.
[2] Woo EM, Wu PL, Chiang CP, Liu HL. Macromol Rapid Commun 2004; 25:942.
[3] Ghosh AK, Woo EM, Sun YS, Lee LD, Wu MC. Macromolecules 2005; 38:4780.
[4] Hall IH, Ibrahim BA. Polymer 1982;23:805.
[5] Palmer A, Poulin-Dandurand S, Revol JF, Brisse F. Eur Polym J 1984;20: 783.
[6] Brisse F, Palmer A, Moss B, Dorset D, Roughead A, Miller DP. Eur Polym J 1984;20:791.
[7] Wu MC, Woo EM, Yoshioka T, Tsuji M. Polymer 2006;47:5523.
[8] Medellín-Rodríguez FJ, Phillips PJ, Lin JS. Macromolecules 1996;29: 7491.
[9] Woo EM, Ko TY. Colloid Polym Sci 1996;274:309.
[10] Wang ZG, Hsiao BS, Sauer BB, Kampert WG. Polymer 1999;40:4615.
[11] Wang ZG, Hsiao BS, Fu BX, Liu L, Yeh F, White H, et al. Polymer 2000; 41:1791.
[12] Wu PL, Woo EM. J Polym Sci Polym Phys 2002;40:1571.
[13] Ivanov DA, Hocquet S, Dosière M, Koch MHJ. Eur Phys J E 2004;13:363.
[14] Stein RS, Misra A. J Polym Sci Polym Phys Ed 1980;18:327.
[15] Yeh JY, Runt J. J Polym Sci Polym Phys 1989;27:1543.
[16] Runt J, Miley DM, Zhang X, Gallagher KP, McFeaters K, Fishburn J. Macromolecules 1992;25:1929.
[17] Righetti MC. Thermochim Acta 1999;330:131.
[18] Hsiao BS, Wang ZG, Yeh FJ, Gao Y, Sheth K. Polymer 1999;40:3515.
[19] Hall IH, Pass MG, Rammo NN. J Polym Sci Polym Phys Ed 1978;16:1409.
[20] Hall IH, Rammo NN. J Polym Sci Polym Phys Ed 1978;16:2189.
[21] Keller A, Cheng SZD. Polymer 1998;39:4461.
[22] Cheng SZD, Keller A. Annu Rev Mater Sci 1998;28:553.
[23] Chu B, Hsiao BS. Chem Rev 2001;101:1727.
[24] Fischer EW. Pure Appl Chem 1971;26:385.
[25] Belbéoch B, Guinier A. Makromol Chem 1959;31:1.
[26] O'Leary K, Geil PH. J Macromol Sci Phys 1967;B1:147.
[27] Pope DP, Keller A. J Polym Sci Polym Phys Ed 1976;14:821.
[28] Crist B. J Polym Sci Polym Phys 2001;39:2454.
[29] Crist B. Macromolecules 2003;36:4880.
[30] Stribeck N, Ruland W. J Appl Crystallogr 1978;11:535.
[31] Stribeck N. Colloid Polym Sci 1993;271:1007.
[32] Gilbert M, Hybart FJ. Polymer 1972;13:327.
[33] Wu PL. Ph.D. thesis. Department of Chemical Engineering, National Cheng Kung University, Tainan, Taiwan; 2003.
[34] Lai YH, Sun YS, Jeng U, Huang YS, Song YF, Tsang KL, et al. Nucl Instrum Methods Phys Res Sect B 2005;238:205.
[35] Strobl GR, Schneider M. J Polym Sci Polym Phys Ed 1980;18:1343.
[36] Strobl GR, Schneider M, Voigt-Martin IG. J Polym Sci Polym Phys Ed 1980;18:1361.
[37] Santa-Cruz C, Stribeck N, Zachmann HG, Baltá Calleja FJ. Macromolecules 1991;24:5980.
[38] Albrecht T, Strobl G. Macromolecules 1996;29:783.
[39] Ruland W. J Appl Crystallogr 1971;4:70.
[40] Ruland W. Colloid Polym Sci 1977;255:417.
[41] Barnes JD, Kolb R, Barnes K, Nakatani AI, Hammouda B. J Appl Crystallogr 2000;33:758.
[42] Hosemann R, Bagchi SN. Direct analysis of diffraction by matter. Amsterdam: North-Holland; 1962.
[43] Richter D, Schneiders D, Monkenbusch M, Willner L, Fetters LJ, Huang JS, et al. Macromolecules 1997;30:1053.
[44] Schmidtke J, Strobl G, Thurn-Albrecht T. Macromolecules 1997;30: 5804.
[45] Schultz JM, Lin JS, Hendricks RW. J Appl Crystallogr 1978;11:551.
[46] Schultz JM, Fischer EW, Schaumburg O, Zachmann HA. J Polym Sci Polym Phys Ed 1980;18:239.
[47] Vonk CG, Koga Y. J Polym Sci Polym Phys Ed 1985;23:2539.
[48] Rule RJ, Liggat JJ. Polymer 1995;36:3831.
[49] Denchev Z, Nogales A, Šics I, Ezquerra TA, Baltá-Calleja FJ. J Polym Sci Polym Phys 2001;39:881.
[50] Hsiao BS, Gardner KH, Wu DQ, Chu B. Polymer 1993;34:3996.
[51] Verma R, Marand H, Hsiao BS. Macromolecules 1996;29:7767.
[52] Fougnies C, Damman P, Dosière M, Koch MHJ. Macromolecules 1997; 30:1392.
[53] Hsiao BS, Ho RM, Cheng SZD. J Polym Sci Polym Phys 1995;33:2439.
[54] Denchev Z, Nogales A, Ezquerra TA, Fernandes-Nascimento J, Baltá-Calleja FJ. J Polym Sci Polym Phys 2000;38:1167.
[55] Sperling LH. Introduction to physical polymer science. New York: John Wiley & Sons; 1993.